Frequency Control by BESS for Smooth Island Transition of Hydro-Powered Microgrid

Ahmed Sunjaq, Peiyuan Chen, Massimo Bongiorno, Ritwik Majumder, and Jan R Svensson

***Abstract*—This paper develops the frequency controller for a battery energy storage system (BESS) to facilitate a smooth island transition of a hydro-powered microgrid during an unplanned grid outage. The proposed frequency controller uses a PI-based droop structure. The analytical expression of the controller parameter tuning is derived that accounts for the limitations in the power response of a hydro generator and the desired frequency performance criteria set by the microgrid operator. The effectiveness of the frequency controller tuning was verified in Simulink using phasor simulations. Results show that the proposed PI-based droop outperforms the classical proportional droop control in order to fulfil the frequency quality requirement of the microgrid without over-dimensioning the size of the storage capacity.**

***Index Terms*—BESS, hydro turbine, coordination, industrial microgrid, island transition, frequency control, frequency nadir.**

I. Introduction

Commercial and industrial (C&I) facilities are critical loads requiring high degree of reliability and resiliency [1]. Although the grid operator is entitled to provide its consumers with N-1 supply reliability, this is still not adequate for C&I facilities, especially in areas subject to frequent extreme weather conditions. Thus, most C&I facilities have their own local backup gas or diesel generators to supply their critical loads in case of grid outage. However, this generation type is not environmentally friendly, and many C&I facilities have set their own targets for reducing CO2 emissions. One solution is to replace the backup generation with a battery energy storage system (BESS). However, lengthy outage requires large storage capacity, which becomes uneconomical for C&I facility owners.

In Sweden, many C&I facilities are located close to a river where hydro generators are installed. Paper and pulp factories are sensitive to grid disturbances and may take several days to recover from even brief interruption [2]. For instance, a paper and pulp factory is supplied from the same substation to which a hydro-power plant in a close-by river is connected. Another example is the ongoing Ludvika microgrid project in Sweden, where hydro generators will power the local community if an outage occurs in the upstream grid [3]. For unplanned disconnections from the upstream grid, hydro generators need the ability to quickly regulate their power output and thus ensure continuous operation of a facility. This allows them to maintain local frequencies and voltages within acceptable limits. However, limitations exist in the frequency support capability of a hydro turbine. First, the maximum opening/closing speed of the wicket gate is limited, especially when the upper reservoir water level is low [4]. This limits the ramp rate for fast frequency regulation. Second, the penstock length increases the time delay for water to reach its steady flow rate when opening/closing the wicket gate. The delay caused by the penstock may further limit the power response from a hydro turbine when it undergoes a frequency disturbance, or even trigger oscillations in the frequency response [5]. To shorten the effective penstock length, a surge tank with a small water reservoir can be located close to the turbine. However, unwanted oscillations between the surge tank and upper reservoir may occur and bring about slow frequency oscillations [6]. Third, when changing the direction of the wicket gate position, the gears briefly lose contact with each other, which may cause sustained frequency oscillations known as the backlash problem. [7].

To overcome the foregoing limitations of hydro turbines, fast-acting devices such as a BESS of limited storage capability can be deployed to assist the frequency regulation of a microgrid [8]. In fact, many C&I facilities already have BESS installed to provide temporary power supply before their own backup generators cut in [1].

Fig. 1 summarises the available strategies for controlling BESS in both grid-connected mode and island operation mode [9]–[14]. The control strategies include the synchronization method, active power and/or frequency controllers and reactive power and/or voltage controllers. The common practice during grid-connected mode is to have the BESS as standby with active power control for synchronization and with reactive power control. Once the loss of main is detected, the typical approach is to switch to open-loop voltage control. Thus, the smooth transition between the two operational modes depends on both the speed of island detection and the control strategies adopted for them. However, limited literature is available on how to coordinate the control between hydro generators and BESSs for grid frequency regulation. Reference [15] proposes a high-pass filter based frequency controller for the BESS to provide fast frequency support to a transmission grid with reduced synchronous inertia. However, the high-pass filter is not sufficient if the BESS is desired to provide sustained frequency reserve, such as in microgrid applications. Furthermore, the parameter turning of the high-pass filter in [15] does not account for the desired system frequency performance criteria. A dynamic virtual power plant design is proposed in [16] that coordinates the control between hydro and BESS to provide a frequency containment reserve (FCR) to the grid. The frequency controller for the BESS is designed to be a 4^{th}-order system while assuming a perfect knowledge of a simple hydro turbine model. The frequency controller may

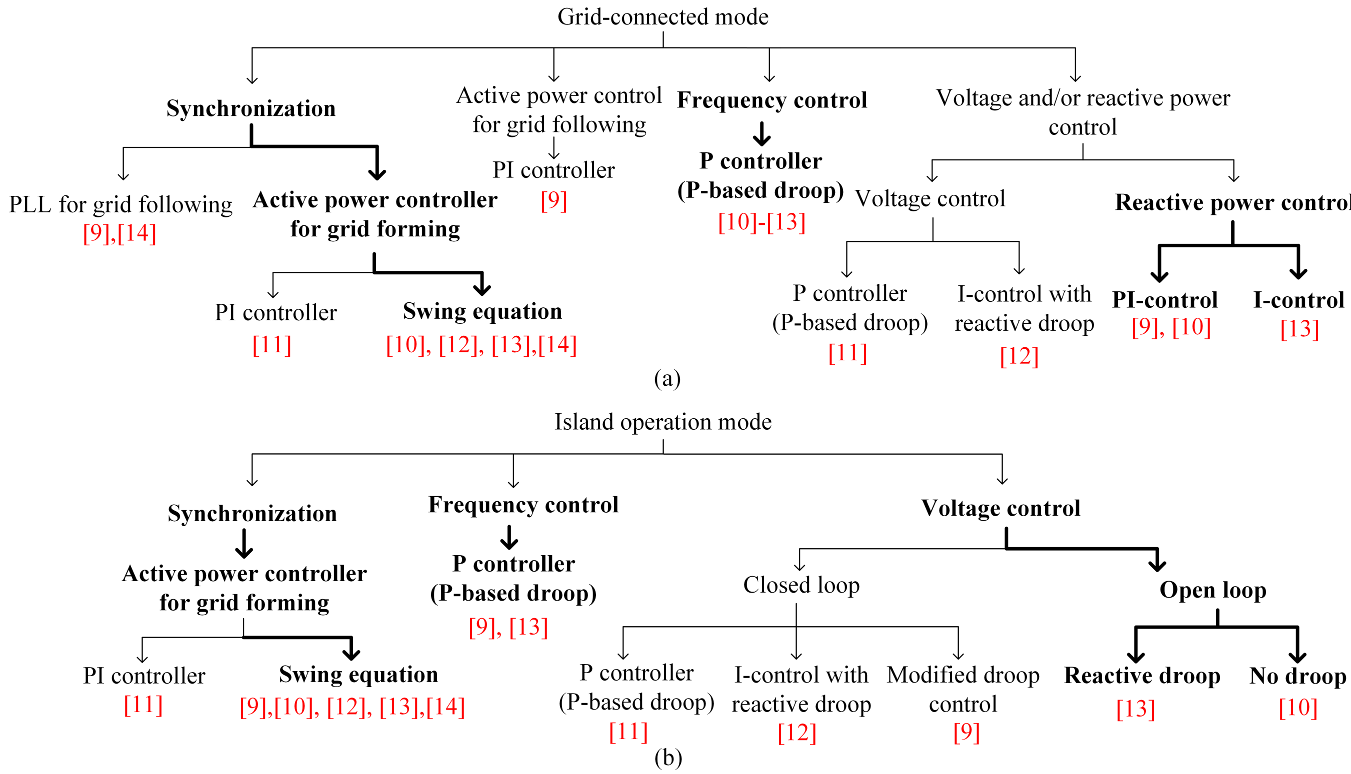

Fig. 1: Overview of synchronization, active power and frequency, reactive power and voltage control of BESS during grid-connected mode and island-operation mode. Commonly used BESS control strategies are highlighted in bold. P controller refers to proportional controller, I controller refers to integral controller and PI refers to both.

become even more complex if a more detailed turbine model is used.

Thus, this paper aims to develop an efficient frequency control strategy for BESS to facilitate the unplanned island transition of a hydro-powered microgrid by accounting for the limitations in the hydro turbines and the desired frequency performance criteria of the microgrid. The main contributions of the paper include:

- PI-based droop frequency control strategy for BESS, accounting for the technical limitations of hydro power plants in facilitating microgrid island transition and microgrid frequency performance criteria,
- Corresponding analytical expressions for tuning the PI-based droop controller.

II. Microgrid Model for Island Transition Studies

A. Electrical diagram of microgrid

Fig. 2 shows the electrical diagram of a medium-voltage distribution system to be operated as a microgrid in the west coast of Sweden. The paper and pulp factory is supplied from a 140/11 kV substation, to which a hydro power plant is also connected. To enable a smooth island transition of the microgrid, a BESS is installed at the factory.

B. Hydro turbine with governor and exciter model

Fig. 3 shows a generic Francis hydro turbine model with a governor used to provide FCR [17]. The automatic voltage

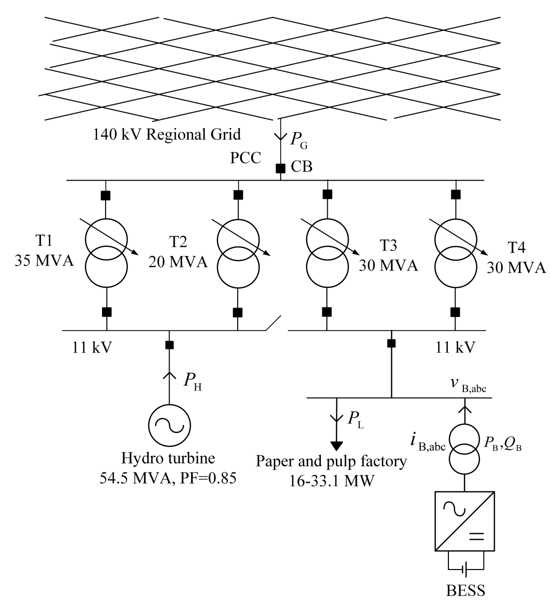

Fig. 2: Hydro-powered microgrid equipped with a BESS to facilitate the smooth island transition of a paper and pulp facility.

controller (AVR) of the hydro generator is implemented as a standard PI controller with a static exciter model typically used in the Nordic 32 power system model [18]. As the paper focuses on the frequency regulation, a detailed description of the AVR and the exciter model will not be included, but can be found in [18].

Based on the frequency deviation signal, the governor sends a reference position for the wicket gate opening. The actuator regulates the guide vanes of the wicket gate. The vanes have maximum/minimum opening positions corresponding to the available reserve for up/down regulation. Moreover, a limit is imposed on the maximum ramp rate of the vanes' opening/closing speed. The water dynamics through the penstock are represented by a lead-lag compensator.

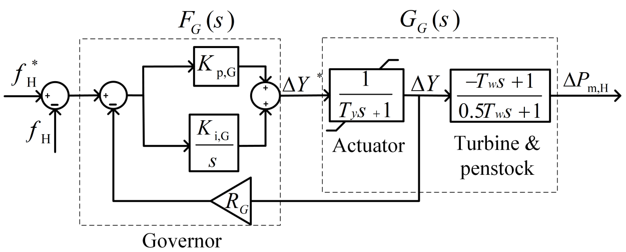

Fig. 3: Simplified model of a Francis hydro turbine and governor for the provision of FCR.

Assuming that the actuator dynamic is much faster than the governor control loop, i.e. $\Delta Y \approx \Delta Y^*$, the governor model may be simplified as displayed in Fig. 4 (a). Such a proportional-integral-based (PI-based) droop governor is equivalent to the summation of a high-pass filter and a low-pass filter as shown in Fig. 4 (b). The relationship of the parameters for the two models is:

$$T_{\mathrm{G}} = \frac{1 + R_{\mathrm{G}} K_{\mathrm{p,G}}}{R_{\mathrm{G}} K_{\mathrm{i,G}}}, \tag{1a}$$

$$K_{\mathrm{tr,G}} = \frac{K_{\mathrm{p,G}}}{1 + R_{\mathrm{G}} K_{\mathrm{p,G}}}, \tag{1b}$$

$$K_{\mathrm{ss,G}} = \frac{1}{R_{\mathrm{G}}}. \tag{1c}$$

For hydro turbines, typically $K_{\mathrm{p,G}} \ll \frac{1}{R_{\mathrm{G}}}$ (for stability reasons), resulting in $K_{\mathrm{tr,G}} \approx K_{\mathrm{p,G}} \ll K_{\mathrm{ss,G}}$ according to (1b) and (1c). The coordination between hydro and BESS for frequency control provision is better interpreted using the model in Fig. 4 (b), as will be demonstrated in Section III-C. The open-loop transfer function of the output mechanical power with respect to the input frequency deviation of the hydro turbine is:

$$\begin{aligned} \frac{\Delta P_{\mathrm{m,H}}}{-\Delta f_{\mathrm{H}}} = & \left(K_{\mathrm{tr,G}} \frac{T_{\mathrm{G}} s}{T_{\mathrm{G}} s + 1} + K_{\mathrm{ss,G}} \frac{1}{T_{\mathrm{G}} s + 1} \right) \\ & \left(\frac{1}{T_{\mathrm{y}} s + 1} \right) \left(\frac{-T_{\mathrm{w}} s + 1}{0.5 T_{\mathrm{w}} s + 1} \right), \end{aligned} \tag{2}$$

where $\Delta f_{\mathrm{H}} = f_{\mathrm{H}} - f_{\mathrm{H}}^*$.

C. Control of BESS

Fig. 5 shows the control diagram of the BESS, including the frequency controller, the active power controller for synchronization, the reactive power controller and the inner vector current controller.

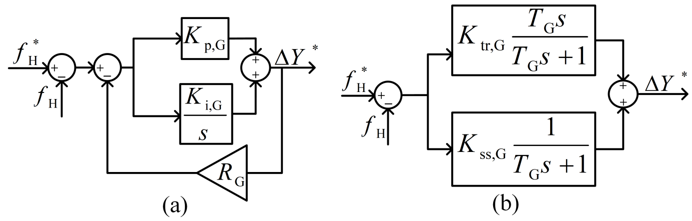

Fig. 4: Two equivalent models of hydro governor: (a) PI-based droop and (b) high-pass filter plus low-pass filter.

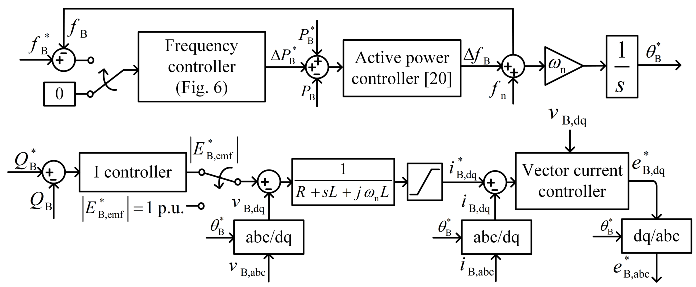

Fig. 5: BESS control strategy used in this paper. The switching from grid-connected mode (default) to island operation mode is indicated by the arrows. R and L in the figure refer to the converter total resistance and inductance, which includes the physical filter and transformer in addition to virtual values.

1) Frequency controller: in contrast to the classical proportional droop controller, this paper proposes a frequency controller using a PI-based droop for the BESS. Fig 6 (a) shows the structure of the PI-based droop controller, which is similar to that of the hydro governor, except that the droop feedback is subtracted from the integrator input only but not from the input to the proportional gain. The BESS frequency controller is also mathematically equivalent to the sum of a high-pass filter and a low-pass filter, as presented in Fig. 6 (b), but with the following equivalent parameters:

$$T_{\mathrm{fc}} = \frac{1}{R_{\mathrm{fc}} K_{\mathrm{i,fc}}}, \tag{3a}$$

$$K_{\mathrm{tr,fc}} = K_{\mathrm{p,fc}}, \tag{3b}$$

$$K_{\mathrm{ss,fc}} = \frac{1}{R_{\mathrm{fc}}}. \tag{3c}$$

One advantage of moving the droop feedback according to Fig. 6 (a) as compared to Fig. 4 (a), is that the transient gain in (3b) can also be larger than the steady state gain in (3c), $K_{\mathrm{tr,fc}} > K_{\mathrm{ss,fc}}$, which is desirable in the case of controlling the BESS. The corresponding open-loop transfer function of the output reference electrical power ΔP_{B}^* of the BESS with respect to its frequency deviation is:

$$\frac{\Delta P_{\mathrm{B}}^*}{-\Delta f_{\mathrm{B}}} = \left(K_{\mathrm{tr,fc}} \frac{T_{\mathrm{fc}} s}{T_{\mathrm{fc}} s + 1} + K_{\mathrm{ss,fc}} \frac{1}{T_{\mathrm{fc}} s + 1} \right), \tag{4}$$

where $\Delta f_{\mathrm{B}} = f_{\mathrm{B}} - f_{\mathrm{B}}^*$.
Hereby in this paper, the term "governor" refers to the frequency-control action executed by the hydro turbine while the term "frequency controller" is reserved for the BESS.

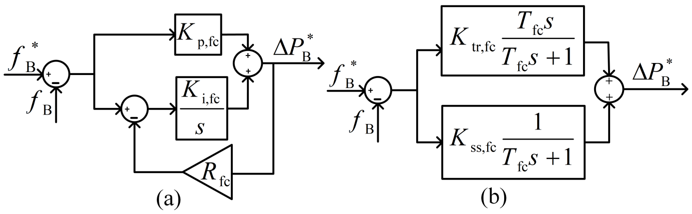

Fig. 6: Two equivalent models of BESS frequency controller: (a) PI-based droop and (b) high-pass filter plus low-pass filter.

2) Active power controller for synchronization: this paper adopts the active power controller based method to generate the synchronization angle of the BESS. Different controller designs exist, either by emulating the swing equation of a synchronous machine [14], [19] or directly using a PI controller [11], [20]. A detailed comparison on different designs of the active power controller for a grid-forming converter can be found in [20]. This paper adopts the PI controller-based active power controller as described in [20].

3) Current controller: a standard vector current controller (VCC) is adopted to control and limit the converter current. The detailed description of the VCC can be found in [21].

4) Reactive power and voltage control: in this paper, the BESS uses reactive power controller during the grid-connected mode, and switches to the voltage controller during the island mode as shown in Fig. 5.

5) Island detection: a communication-based island detection is used by monitoring the breaker status of the grid infeed line. The communication usually uses Ethernet cable or optical fiber and the communication delay is in the order of a few milliseconds and has little impact on the controller response [22]. A passive island detection method, e.g. based on local frequency measurement, is typically used to handle communication failure [23]. The impact of communication failure will be discussed later.

III. Proposed BESS frequency controller design in a hydro-powered microgrid

A. Criteria and scenarios for smooth island transition

The following two criteria are specified for the microgrid to achieve a smooth island transition:

- maximum instantaneous frequency deviation ($\Delta f^{\max}$).
- maximum steady state frequency deviation ($\Delta f_{\mathrm{ss}}^{\max}$).

Steady state refers here to the period of time after the frequency has stabilised and before the activation of the secondary frequency reserve to restore the frequency to 50 Hz. The need for an additional BESS to ensure a smooth island transition depends significantly on the characteristics of the hydro turbine and its frequency regulation capability. If the hydro is not equipped with governor, then only the BESS controls the microgrid frequency during island transition. In this case, the typical approach is to use a P controller (P-based droop), as the response of the BESS is very fast. This controller is straightforward and discussed extensively in the literature [10]–[13], and thus will not be further explained. In the following subsections, the scenario in which the hydro is equipped with a governor will be further explored.

B. Steady-state power sharing between BESS and hydro

When the hydro is equipped with governor, it provides steady-state frequency reserve according to its droop setting in case of power imbalance during island transition. Two cases are considered here, depending on whether the hydro has sufficient reserve to cover the largest power imbalance.

1) BESS and hydro share steady-state reserve: in this case, the steady-state frequency deviation when using both BESS and hydro to provide droop-based frequency control is given by [24],

$$\Delta f_{\mathrm{ss}} = \frac{-\Delta P_{\mathrm{dm}}}{\frac{1}{R_{\mathrm{G}}} + \frac{1}{R_{\mathrm{fc}}} + D_{\mathrm{L}}}, \tag{5}$$

where ΔP_{dm} is the dimensioning disturbance and D_{L} is the load frequency dependence. The BESS should provide additional reserve power in steady state if the hydro does not have sufficient regulation strength ($\frac{1}{R_{\mathrm{G}}}$) to meet the desired $\Delta f_{\mathrm{ss}}^{\max}$, i.e.

$$\frac{1}{R_{\mathrm{G}}} < \frac{-\Delta P_{\mathrm{dm}}}{\Delta f_{\mathrm{ss}}^{\max}} - D_{\mathrm{L}} = \left|\frac{\Delta P_{\mathrm{dm}}}{\Delta f_{\mathrm{ss}}^{\max}}\right| - D_{\mathrm{L}} \tag{6}$$

where $-\Delta P_{\mathrm{dm}}/\Delta f_{\mathrm{ss}}^{\max}$ is positive since the disturbance and the frequency deviation are always opposite in sign. The BESS regulation strength ($\frac{1}{R_{\mathrm{fc}}}$) is obtained by (5) such that the frequency deviation in steady state does not exceed $\Delta f_{\mathrm{ss}}^{\max}$, i.e.

$$K_{\mathrm{ss,fc}} = \frac{1}{R_{\mathrm{fc}}} = \frac{-\Delta P_{\mathrm{dm}}}{\Delta f_{\mathrm{ss}}^{\max}} - \frac{1}{R_{\mathrm{G}}} - D_{\mathrm{L}}. \tag{7}$$

One assumption made here is that $D_{\mathrm{L}} < \left|\frac{\Delta P_{\mathrm{dm}}}{\Delta f_{\mathrm{ss}}^{\max}}\right|$. If $D_{\mathrm{L}} \geq \left|\frac{\Delta P_{\mathrm{dm}}}{\Delta f_{\mathrm{ss}}^{\max}}\right|$, then there is no need for the BESS to provide frequency control, as the load frequency dependence can maintain the frequency nadir within the limits.

2) Only hydro provides steady-state reserve: if the hydro has sufficient regulation strength, i.e

$$\frac{1}{R_{\mathrm{G}}} \geq \left|\frac{\Delta P_{\mathrm{dm}}}{\Delta f_{\mathrm{ss}}^{\max}}\right| - D_{\mathrm{L}}, \tag{8}$$

there is no need for the BESS to provide steady-state reserve, i.e. $K_{\mathrm{ss,fc}} = 0$. In this case, the frequency controller in Fig. 6 (b) is reduced to a high-pass filter with a transient gain of $K_{\mathrm{tr,fc}}$ (HF-based).

C. Proposed dynamic power coordination

Due to the non-minimum phase response of the hydro turbine and slow response of water penstock, the hydro has poor dynamic performance when regulating frequency alone in a microgrid. To fulfil the maximum allowed instantaneous frequency deviation of the microgrid operation, a BESS is deployed to assist the hydro generator in regulating the frequency of the microgrid.

1) Design of transient gain of BESS ($K_{\mathrm{tr,fc}}$): the transient gain of the BESS frequency controller is tuned such that, with the hydro, they can maintain the frequency above the minimum allowed frequency nadir during transients. Fig. 7 shows the bode diagram of hydro (solid blue curve) and BESS (solid green curve) according to (2) and (4), respectively. The dashed blue curve corresponds to the same transfer function as in (2) but neglects the actuator and penstock dynamics. As shown in the upper figure, the transient gain $K_{\mathrm{tr,G}}$ of the hydro governor (dashed blue curve) is typically set to 1-10 p.u. [17]. However, as shown in the solid blue curve in the bottom figure, during the transient response (frequency components above $1/T_{\mathrm{G}}$ rad/s), the delay introduced by the actuator and penstock becomes dominant. Therefore, achieving the requirement of limiting the maximum frequency deviation to $\Delta f^{\max}$ while taking into consideration the delays of the hydro turbine is desired. To achieve this goal, the total transient gain of the hydro and the BESS is designed according to

$$K_{\mathrm{tr,tot}} \geq -\frac{\Delta P_{\mathrm{dm}} + D_{\mathrm{L}}\Delta f^{\max}}{\Delta f^{\max}}.$$

The total transient gain is obtained as the summation of (2) and (4), where $s \to j\infty$, which gives $K_{\mathrm{tr,tot}} = K_{\mathrm{tr,fc}}$. This design implies that the transient gain of the BESS frequency controller is responsible for limiting the frequency nadir and it should not be less than

$$K_{\mathrm{tr,fc}} = -\frac{\Delta P_{\mathrm{dm}} + D_{\mathrm{L}}\Delta f^{\max}}{\Delta f^{\max}}. \quad (9)$$

The transient gain is desired to be larger than or equal to the steady steady gain, i.e. $K_{\mathrm{tr,fc}} \geq K_{\mathrm{ss,fc}}$. Unlike hydro generators, there is no need to set BESS' transient gain to be less than its steady state gain because of the very fast power response of the BESS. In case $K_{\mathrm{tr,fc}} = K_{\mathrm{ss,fc}}$, the BESS frequency controller reduces to a P-based droop according to Fig. 6 (b).

2) Design of frequency controller time constant (T_{fc}): the BESS frequency controller has a dynamic gain that changes from $K_{\mathrm{tr,fc}}$ to $K_{\mathrm{ss,fc}}$ following a disturbance (see Fig. 6 (b)). The time that takes for the gain to change depends on T_{fc}. As described in the previous subsection, the BESS has a transient gain equal to or larger than its steady-state gain. In contrast, hydro typically has a transient gain smaller than its steady-state gain instead. A critical case for coordination between hydro and BESS is when the BESS has a steady-state gain much smaller than its transient gain (opposite to hydro). In this case, tuning the BESS controller time constant to be too small will cause a too fast reduction in its dynamic gain from $K_{\mathrm{tr,fc}}$ to $K_{\mathrm{ss,fc}}$, which may result in lack of frequency support to the microgrid. On the other hand, tuning the time constant to be too large will result in an over dimension of the storage capacity of the BESS. It is, thus, important to tune the frequency controller time constant properly. The tuning of the BESS frequency controller time constant is also divided into two cases, depending on whether the hydro has sufficient reserve to cover the largest power imbalance.

a) BESS and hydro share steady-state reserve ($\frac{1}{R_{\mathrm{G}}} < \left|\frac{\Delta P_{\mathrm{dm}}}{\Delta f_{\mathrm{ss}}^{\max}}\right| - D_{\mathrm{L}}$): according to (7) and (9) for the BESS frequency controller, the break-even point at which $K_{\mathrm{tr,fc}} = K_{\mathrm{ss,fc}}$ is when

$$\frac{1}{R_{\mathrm{G}}} = |\Delta P_{\mathrm{dm}}| \left(\frac{1}{|\Delta f_{\mathrm{ss}}^{\max}|} - \frac{1}{|\Delta f^{\max}|} \right). \quad (10)$$

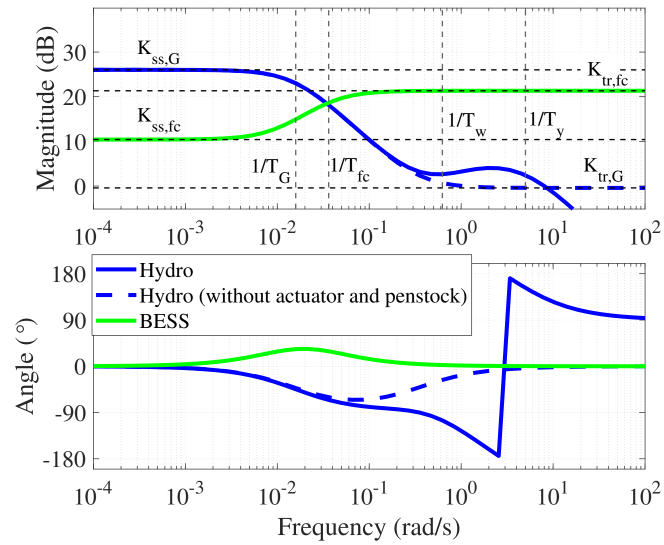

Fig. 7: Bode magnitude plot (top) and bode phase plot (bottom) of hydro and BESS according to the transfer functions given by (2) and (4), respectively.

i) $\frac{1}{R_{\mathrm{G}}} \leq |\Delta P_{\mathrm{dm}}| \left(\frac{1}{|\Delta f_{\mathrm{ss}}^{\max}|} - \frac{1}{|\Delta f^{\max}|} \right)$

This case arises when the hydro provides a relatively small amount of reserve in steady state, while the BESS provides a relatively high amount of reserve in steady state. In this case, the transient gain is set equal to the steady-state gain. Thus, the controller reduces to a P-based droop and the time constant T_{fc} is not needed.

ii) $|\Delta P_{\mathrm{dm}}| \left(\frac{1}{|\Delta f_{\mathrm{ss}}^{\max}|} - \frac{1}{|\Delta f^{\max}|} \right) < \frac{1}{R_{\mathrm{G}}} < \left|\frac{\Delta P_{\mathrm{dm}}}{\Delta f_{\mathrm{ss}}^{\max}}\right| - D_{\mathrm{L}}$

This case arises when hydro provides a relatively high amount of reserve in steady state, while the BESS provides a relatively small amount of reserve in steady state. In this case, since the transient gain $K_{\mathrm{tr,fc}}$ is higher than the steady-state gain $K_{\mathrm{ss,fc}}$, the tuning of the BESS's time constant is crucial in fulfilling the smooth island transition requirement. Since the hydro governor bandwidth is at much lower frequency as compared to penstock and actuator dynamics (see Fig. 7), the dynamics of the subsequent ones may be neglected when designing the BESS frequency controller time constant. Thus, the hydro transfer function in (2) is simplified to:

$$\frac{\Delta P_{\mathrm{m,H}}}{-\Delta f_{\mathrm{H}}} \approx K_{\mathrm{tr,G}} \frac{T_{\mathrm{G}} s}{T_{\mathrm{G}} s + 1} + K_{\mathrm{ss,G}} \frac{1}{T_{\mathrm{G}} s + 1}. \quad (11)$$

The resulting unit step responses of the open-loop transfer function (11) for the hydro and (4) for the BESS are, respectively:

$$K_{\mathrm{G}}(t) = -\Delta K_{\mathrm{G}} e^{-\frac{t}{T_{\mathrm{G}}}} + K_{\mathrm{ss,G}}, \tag{12a}$$

$$K_{\mathrm{fc}}(t) = \Delta K_{\mathrm{fc}} e^{-\frac{t}{T_{\mathrm{fc}}}} + K_{\mathrm{ss,fc}}, \tag{12b}$$

where $\Delta K_{\mathrm{G}} = K_{\mathrm{ss,G}} - K_{\mathrm{tr,G}}$ and $\Delta K_{\mathrm{fc}} = K_{\mathrm{tr,fc}} - K_{\mathrm{ss,fc}}$. The minimum required frequency controller time constant to achieve a smooth island transition is obtained by assuming that the summation of the governor gain, given by (12a), and frequency controller gain, given by (12b), should be monotonically increasing, i.e:

$$\frac{d}{dt}(K_{\mathrm{tot}}(t)) \geq 0, \tag{13}$$

where $K_{\mathrm{tot}}(t) = K_{\mathrm{fc}}(t) + K_{\mathrm{G}}(t)$. The total open-loop response is expressed as the summation of (12a) and (12b), i.e:

$$K_{\mathrm{tot}}(t) = \Delta K_{\mathrm{fc}} e^{-\frac{t}{T_{\mathrm{fc}}}} - \Delta K_{\mathrm{G}} e^{-\frac{t}{T_{\mathrm{G}}}} + K_{\mathrm{ss,tot}}, \tag{14}$$

where $K_{\mathrm{ss,tot}} = K_{\mathrm{ss,fc}} + K_{\mathrm{ss,G}}$. The first-order Taylor series expansion of (14) gives:

$$\begin{aligned} K_{\mathrm{tot}}(t) &\approx K_{\mathrm{tot}}(t=0) + \frac{dK_{\mathrm{tot}}(t)}{dt}\Big|_{t=0} t \\ &= \Delta K_{\mathrm{fc}}(1 - \frac{1}{T_{\mathrm{fc}}}t) - \Delta K_{\mathrm{G}}(1 - \frac{1}{T_{\mathrm{G}}}t) + K_{\mathrm{ss,tot}}. \end{aligned} \tag{15}$$

Applying the condition in (13) to (15), the minimum time constant of the BESS frequency controller obtained is

$$T_{\mathrm{fc}} = \frac{\Delta K_{\mathrm{fc}}}{\Delta K_{\mathrm{G}}} T_{\mathrm{G}} = \frac{K_{\mathrm{tr,fc}} - K_{\mathrm{ss,fc}}}{K_{\mathrm{ss,G}} - K_{\mathrm{tr,G}}} T_{\mathrm{G}}. \tag{16}$$

By substituting (1), (7) and (9) in (16), the time constant becomes:

$$T_{\mathrm{fc}} = \left[1 - R_{\mathrm{G}} \Delta P_{\mathrm{dm}} \left(\frac{1}{\Delta f^{\max}} - \frac{1}{\Delta f^{\max}_{\mathrm{ss}}}\right)\right] \frac{(1 + R_{\mathrm{G}} K_{\mathrm{p,G}})^2}{R_{\mathrm{G}} K_{\mathrm{i,G}}}. \tag{17}$$

b) Only hydro provides steady-state power ($\frac{1}{R_{\mathrm{G}}} \geq |\frac{\Delta P_{\mathrm{dm}}}{\Delta f^{\max}_{\mathrm{ss}}}| - D_{\mathrm{L}}$): this case arises when hydro provides the total reserve in steady state, whereas BESS provides no reserve in steady state ($K_{\mathrm{ss,fc}} = 0$). By substituting (1) and (9) in (16), the time constant becomes:

$$T_{\mathrm{fc}} = -\frac{\Delta P_{\mathrm{dm}} + D_{\mathrm{L}} \Delta f^{\max}}{\Delta f^{\max}} \frac{(1 + R_{\mathrm{G}} K_{\mathrm{p,G}})^2}{K_{\mathrm{i,G}}}. \tag{18}$$

Fig. 8 summarises all the scenarios, plus the corresponding tuning of the BESS frequency controller illustrated in this section.

IV. Microgrid Case Study

A. Performance criteria, load and hydro parameters

Table I lists the performance criteria data described in Section III-A, the load frequency dependence and the hydro model parameters depicted in Fig. 3 and 4. H_{H} refers to the hydro inertia constant. The minimum allowed frequency nadir is set to 49 Hz ($\Delta f^{\max} = -1$ Hz) [2]. The base power is chosen to be the rated active power (46.3 MW) of the hydro generator.

TABLE I: Performance criteria, load and hydro parameters [17], [25].

$\Delta f^{\max}$	-0.02 p.u. (-1 Hz)	$K_{\mathrm{ss,G}}$	20 p.u.	H_{H}	3.8 s
$\Delta f^{\max}_{\mathrm{ss}}$	-0.01 p.u. (-0.5 Hz)	$K_{\mathrm{tr,G}}$	0.95 p.u.	T_{y}	0.2 s
D_{L}	0	T_{G}	63 s	T_{w}	1.6 s

B. Steady-state power flow

Fig. 9 shows the time duration curve of the import power from the upstream grid measured in 2018 at a resolution of one hour. The import power exceeds 10.8 MWh/h for 5% of the year which is considered to be the dimensioning disturbance. The local industrial load is assumed to operate at its rated power with a unity power factor (fully compensated), i.e. 33.1 MW, of which 22.3 MW is supplied by the hydro. The hydro turbine has an active power capacity of $54.5\mathrm{MVA} \times 0.85 = 46.3\mathrm{MW}$, with a maximum up-regulation reserve of 24 MW. With a governor droop of 5%, the hydro will provide 9.3 MW of frequency reserve when the microgrid frequency reaches 49.5 Hz in steady state. As D_{L} =0, the BESS needs to provide an additional 1.5 MW (10.8 MW - 9.3 MW) in order to limit the steady-state frequency to 49.5 Hz. Table II summarises the steady-state grid import power P_{G}, hydro power generation P_{H}, BESS power generation P_{B} and microgrid load P_{L}, before and after loss of the main grid. A load of constant power type with no dependency on either the voltage or the frequency is adopted. As both the hydro and the factory are located very close to the substation, no medium voltage cables are modelled.

TABLE II: Steady-state power flow before and after the loss of the main grid.

		Pre-disturbance	Post-disturbance
Grid import	P_{G} (ΔP_{dm})	10.8 MW	0
Hydro	P_{H}	22.3 MW	31.6 MW
BESS	P_{B}	0	1.5 MW
Load	P_{L}	33.1 MW	33.1 MW

C. BESS frequency controller parameters

Fig. 10 (top) shows three different regions of steady-state power sharing between the hydro and the BESS with respect to different hydro governor droop settings. The three different droop regions are denoted by the numericals 1,2 and 3 in Fig. 8. As the hydro droop decreases, it covers larger share of steady-state power as compared to the BESS. Fig. 10 (middle) shows the resulting steady-state frequency deviation $|\Delta f_{\mathrm{ss}}|$. The deviation in Region 3 is lower than the specified

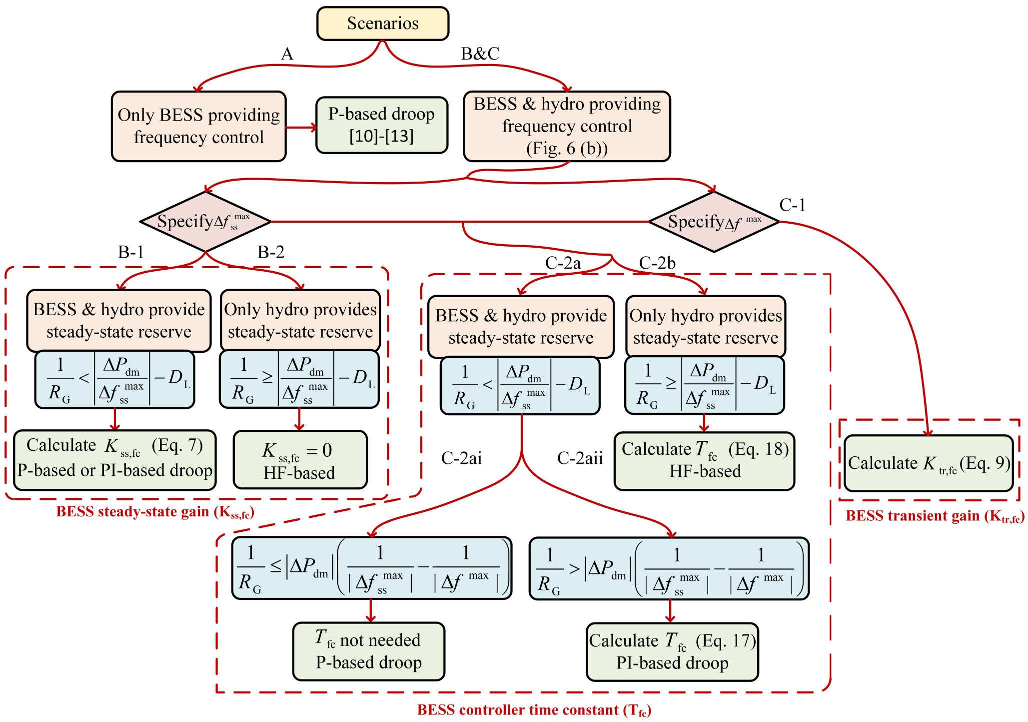

Fig. 8: Flow chart showing the different scenarios and the corresponding BESS frequency controller configuration and tuning.

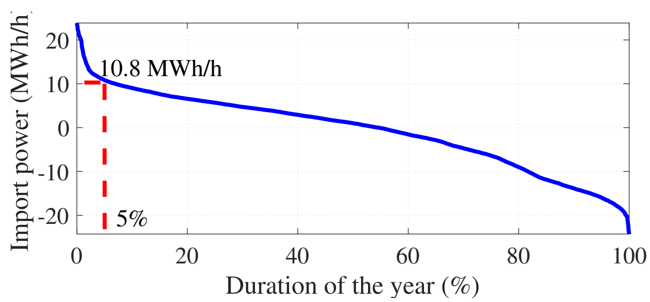

Fig. 9: Time duration curve showing the import active power from the upstream grid over one calender year from 1-1-2018 to 31-12-2018 measured using a resolution of one hour. This data is obtained from local distribution system operator Vattenfall.

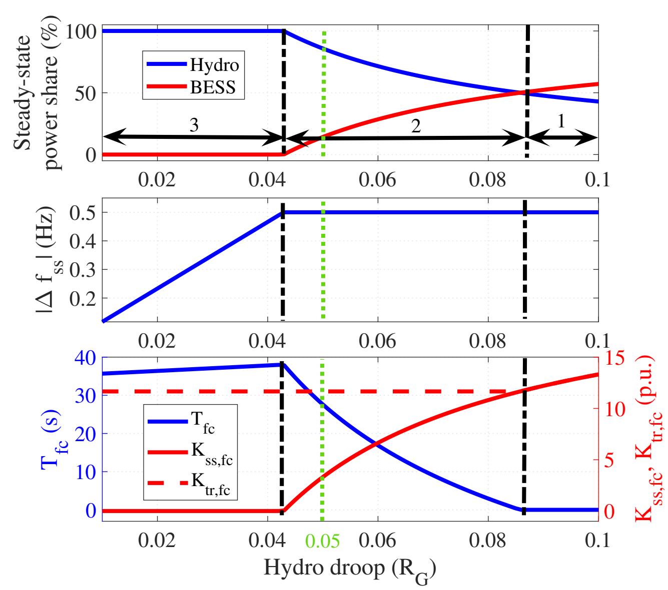

Fig. 10: Impact of hydro droop setting on steady-state power sharing between BESS and hydro (top), steady-state frequency deviation (middle) and BESS frequency controller parameters (bottom). The three different droop regions, 1, 2 and 3, are illustrate in Fig. 8. The choice of tuning is illustrated with the green dotted line.

performance criteria of 0.5 Hz. This is because the hydro droop setting (regulation strength) is very small (high), which limits the steady-state frequency deviation to an even tighter value than required. Fig. 10 (bottom) shows the corresponding three BESS frequency controller parameters, consisting of time constant $T_{\rm fc}$, steady-state gain $K_{\rm ss,fc}$ and transient gain $K_{\rm tr,fc}$. For the following dynamic simulation, the hydro governor droop is set to 5% [17], [25], and the resulting BESS frequency-controller tuning is $T_{\rm fc} = 27.6$ s, $K_{\rm ss,fc} = 3.3$ p.u. and $K_{\rm tr,fc} = 11.7$ p.u. The model is implemented in Matlab/Simulink using phasor simulation.

V. Simulation Results and Discussion

A. PI-based droop vs. P-based droop

Fig. 11 shows a comparison between the P-based and PI-based droop control of the BESS frequency controller in handling the frequency during transients. The upper sub-plot shows the hydro frequency, while the converter frequency is omitted since it has a fast power control loop (5 Hz) and synchronises rapidly with the hydro turbine frequency. The second and the third sub-plots show the change in hydro FCR ($\Delta P_{\rm m,H}$) and the change in BESS frequency reserve (FR) ($\Delta P^{*}_{\rm B}$) respectively. The terms FCR and FR are used to distinguish between the hydro and BESS frequency-based reserves. The grid is disconnected at $t = 5$ s while importing 10.8 MW (0.23 p.u.) of active power. Two different tunings were used for the gain of the P-based control, according to either the steady-state gain (3.3 p.u.) or transient gain (11.7 p.u.). The former case has a poor dynamic performance with a frequency nadir of 47.3 Hz, while the latter case is capable of fulfilling the smooth island transition requirement for the frequency nadir of 49 Hz. However, the latter case requires much greater power in steady state, with a corresponding frequency of 49.6 Hz. This compares to 49.5 Hz in the former case which, based on the requirement, is acceptable. On the other hand, the PI-based droop is preferable to the P-based droop, as it has an additional degree of freedom whereby the transient and steady-state gains can be set independently. Thus, the requirements for both the frequency nadir and the steady-state frequency can be fulfilled using less energy. The secondary frequency control is not implemented here, but after the smooth transition, the hydro's load-set point should be changed to bring the frequency back to 50 Hz, releasing the fast frequency reserve supplied by the BESS.

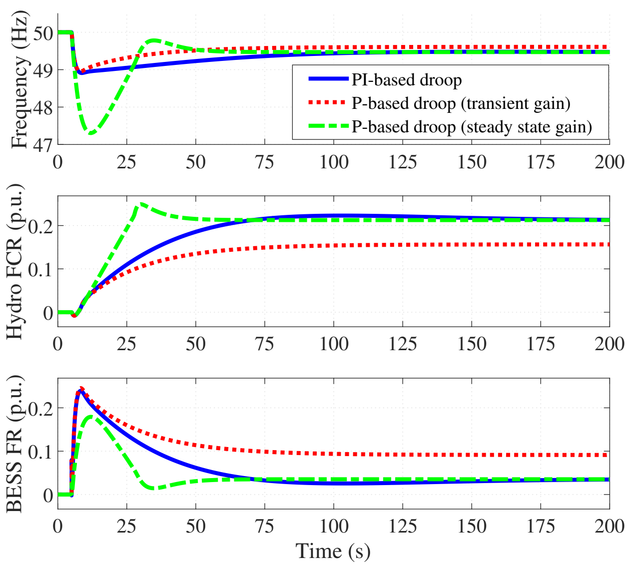

Fig. 11: Impact analysis of BESS frequency controller configuration: hydro frequency response (top), hydro FCR (middle) and BESS FR (bottom).

B. Impact of controller time constant

Fig. 12 shows the impact of the BESS frequency controller time constant tuning on the frequency response. The base value of the controller time constant is 27.6 s (see Section IV-C). With a shorter controller time constant of 5 s, the BESS reduces its FR much quicker than the hydro can increase its FCR. This leads to a poor frequency response with a frequency nadir of 48.45 Hz (which is below the requirement of 49 Hz). On the other hand, a longer controller time constant of 70 s will lead to a longer decay time of BESS FR and, thus, more energy consumption. Fig. 13 shows the gain plots of the hydro and the BESS as defined by (2) and (4) respectively, as well as the sum of the two gains. With a time constant of 5 s, the total gain has a non-monotonic behaviour due to the sharp reduction in BESS gain, which does not agree with the criteria specified in (13).

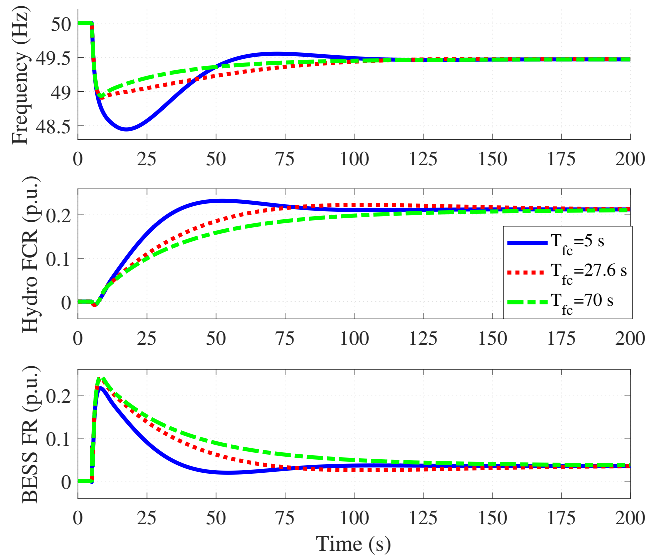

Fig. 12: Impact analysis of BESS frequency controller time constant: hydro frequency response (top), hydro FCR (middle) and BESS FR (bottom).

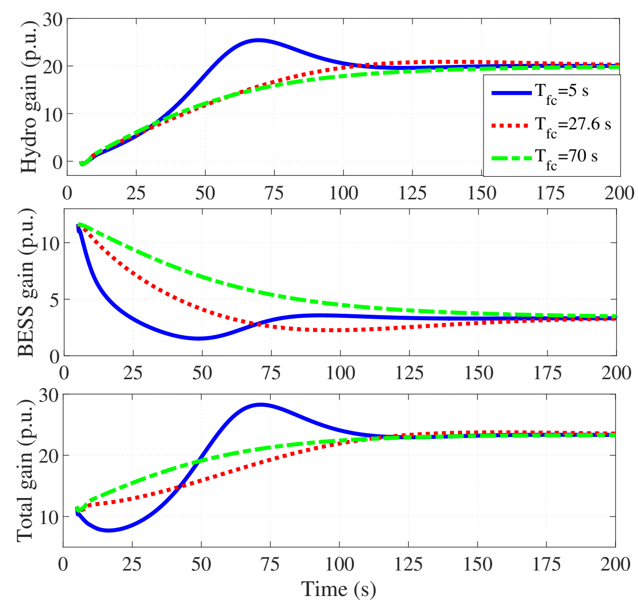

Fig. 13: Impact analysis of BESS frequency controller time constant: hydro gain as given by (2) (top), BESS gain as given by (4) (middle) and total gain of hydro and BESS (bottom).

C. Impact of performance criteria on frequency nadir

Fig. 14 shows the corresponding results when the performance criteria of the minimum allowed frequency nadir is reduced from 49 Hz to 48.5 Hz and to 48 Hz. As the minimum allowed frequency nadir is reduced from 49 Hz to 48.5 Hz, the hydro increases its FCR more quickly due to a larger frequency error signal. This shortens the frequency support duration of the BESS, allowing it to ramp down its power faster. Thus, less energy is required from the BESS. However, by further reducing the minimum allowed frequency nadir to 48 Hz, the reduced energy requirement of the BESS is no longer as significant. This is because the hydro has reached its maximum ramp rate limit. The maximum active power of the BESS is reduced slightly when relaxing the frequency nadir requirements. This is because of the longer time to reach the frequency nadir, which allows more time for the hydro to increase its FCR.

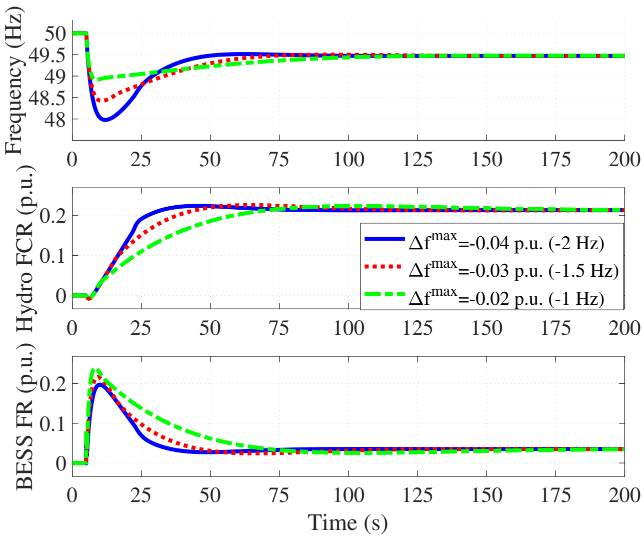

Fig. 14: Impact analysis of maximum allowed frequency deviation: hydro frequency response (top), hydro FCR (middle) and BESS FR (bottom).

VI. Further Discussion

A. Impact of hydro inertia

The coordinated frequency control strategy was also evaluated for lower inertia constant values down to 2.5 s, reflecting the inertia constant of a pelton turbine [26]. In case of reduced synchronous inertia in the microgrid, the absolute value of the initial rate-of-change-of-frequency (RoCoF) has increased but then quickly reduces. This is because the P-controller of the BESS injects power proportionally to the frequency deviation with little time delay. As a consequence, the frequency nadir remains more or less unchanged. In Sweden, there is no RoCoF based protection for generators. However, if it is desired to limit the initial RoCoF, a synthetic inertia can be provided by adjusting the bandwidth of the active power control loop [20].

B. Fall-back solution in case of communication failure

If the grid-tie breaker (breaker CB in Fig. 2) signal of the microgrid should be lost, local measurement signals such as frequency and/or voltage can be used as a backup for island detection. Since the BESS is controlled as a PQ bus before the island condition is detected, microgrid voltage and frequency will start to deviate from their normal ranges. One common passive island detection method is to use the local frequency measurement [23]. If the threshold for the frequency-based island detection method is set to 49 Hz, then the frequency nadir may drop slightly below 49 Hz before the BESS quickly ramps up its power to bring the frequency back to its acceptable limit.

C. Risk of power oscillations

There is no significant power oscillations observed in the cases analysed, even when the distance between the hydro and the BESS is increased to 30 km. One reason is that the power rating of the BESS is about 4.5 times smaller than the hydro generator. Another reason is that the BESS is typically designed to provide a large damping power [14]. However, power oscillations may start to appear if the two power sources of comparable sizes are connected through a long cable and that the BESS is poorly tuned to provide little or no damping as illustrated in [9]. This should definitely be avoided.

VII. Conclusions

This paper has developed a simple yet effective BESS frequency controller to achieve a smooth island transition of a hydro-powered microgrid. The proposed frequency controller uses a PI-based droop. The parameter tuning of the BESS frequency controller accounts for the limitations in the power response of a hydro generator and the desired frequency performance criteria set by the microgrid operator, without over-dimensioning the size of the storage capacity. The storage capacity depends on the time constant of the frequency controller, whereas the power capacity depends on the maximum import/export power of the microgrid. The storage capacity can be further reduced if the frequency nadir requirement is relaxed, provided the maximum ramp rate limit of the hydro turbine is not reached.

References

[1] ”Microgrids for Commercial and industrial facilities,” WBCSD., Geneva, Switzerland, Proj. Rep., 2017.

[2] B. Normark et al., ”Reliability in Sweden’s electricity system,” IVA Royal Swedish Academy of Engineering Sciences., Stockholm, Sweden, Proj. Rep., 2017.

[3] ”Ödrift - ett lager med fossilfri energi.” highvoltagevalley.se. https://www.highvoltagevalley.se/sv-SE/projekt/%C3%B6drift-i-krafttanken-41360184 (accessed Dec. 31, 2021).

[4] C. Platero, J. A. Sanchez, C. Nicolet and Allenbach, ”Hydropower Plants Frequency Regulation Depending on Upper Reservoir Water Level,” in Energies, vol. 12, no. 9, 1637, May 2019.

[5] G. Martínez-Lucas, J. I. Sarasúa, J. Á. Sánchez-Fernández, J. R. Wilhelmi, ”Power-Frequency Control of Hydropower Plants with Long Penstocks in Isolated Systems with Wind Generation,” in Renewable Energy, Vol. 83, pp. 245-255, Nov. 2015.

[6] W. Yang, J. Yang, W. Guo and P. Norrlund, ”Frequency Stability of Isolated Hydropower Plant with Surge Tank Under Different Turbine Control Modes,” in Electric Power Components and Systems, vol. 43, no. 15, pp. 1707-1716.

[7] N. Ung, ”The effects of backlash on the frequency stability in a hydro based power system,” M.S. thesis, School of Elect. Eng and Comp. science., KTH University, Stockholm, Sweden, 2018.

[8] N. Hatziargyriou, H. Asano, R. Iravani and C. Marnay, ”Microgrids,” in IEEE Power and Energy Magazine, vol. 5, no. 4, pp. 78-94, July-Aug. 2007.

[9] M. Ganjian-Aboukheili, M. Shahabi, Q. Shafiee and J. M. Guerrero, ”Seamless Transition of Microgrids Operation From Grid-Connected to Islanded Mode,” in IEEE Transactions on Smart Grid, vol. 11, no. 3, pp. 2106-2114, May 2020.

[10] S. Yazdani, M. Ferdowsi and P. Shamsi, "Internal Model Based Smooth Transition of a Three-Phase Inverter Between Islanded and Grid-Connected Modes," in IEEE Transactions on Energy Conversion, vol. 35, no. 1, pp. 405-415, March 2020.

[11] M. Karimi-Ghartemani, S. A. Khajehoddin, P. Piya and M. Ebrahimi, "Universal Controller for Three-Phase Inverters in a Microgrid," in IEEE Journal of Emerging and Selected Topics in Power Electronics, vol. 4, no. 4, pp. 1342-1353, Dec. 2016.

[12] S. M. Ashabani and Y. A. I. Mohamed, "A Flexible Control Strategy for Grid-Connected and Islanded Microgrids With Enhanced Stability Using Nonlinear Microgrid Stabilizer," in IEEE Transactions on Smart Grid, vol. 3, no. 3, pp. 1291-1301, Sept. 2012.

[13] F. Gao and M. R. Iravani, "A Control Strategy for a Distributed Generation Unit in Grid-Connected and Autonomous Modes of Operation," in IEEE Transactions on Power Delivery, vol. 23, no. 2, pp. 850-859, April 2008.

[14] L. Harnefors, M. Schweizer, J. Kukkola, M. Routimo, M. Hinkkanen and X. Wang, "Generic PLL-Based Grid-Forming Control," in IEEE Transactions on Power Electronics, vol. 37, no. 2, pp. 1201-1204, Feb. 2022.

[15] A. Narula, M. Bongiorno, M. Beza and P. Chen, D. Karlsson, "Coordinated Control of Grid-Forming Converters and Hydro Generators to Enhance Frequency Quality of Future Power System," in Electric Power Systems Research (Accepted).

[16] Björk, Joakim, Karl Henrik Johansson, and Florian Dörfler. "Dynamic virtual power plant design for fast frequency reserves: Coordinating hydro and wind." arXiv preprint arXiv:2107.03087 (2021).

[17] R. Eriksson, N, Modig, A. Westberg. "FCR-N design of requirements," ENTSO-E, Tech. Rep., 2017.

[18] T. Van Cutsem et al., "Test Systems for Voltage Stability Studies," in IEEE Transactions on Power Systems, vol. 35, no. 5, pp. 4078-4087, Sept. 2020

[19] P. Rodriguez, I. Candela, C. Citro, J. Rocabert and A. Luna, "Control of grid-connected power converters based on a virtual admittance control loop," 2013 15th European Conference on Power Electronics and Applications (EPE), 2013.

[20] A. Narula, M. Bongiorno, M. Beza and P. Chen, "Tuning and evaluation of grid-forming converters for grid-support," 2021 23rd European Conference on Power Electronics and Applications (EPE'21 ECCE Europe), 2021.

[21] Y. Gui, X. Wang, F. Blaabjerg and D. Pan, "Control of Grid-Connected Voltage-Source Converters: The Relationship Between Direct-Power Control and Vector-Current Control," in IEEE Industrial Electronics Magazine, vol. 13, no. 2, pp. 31-40, June 2019.

[22] A. Vukojevic and S. Lukic, "Microgrid Protection and Control Schemes for Seamless Transition to Island and Grid Synchronization," in IEEE Transactions on Smart Grid, vol. 11, no. 4, pp. 2845-2855, July 2020.

[23] O. Samuelsson and N. Strath, "Islanding detection and connection requirements," 2007 IEEE Power Engineering Society General Meeting, 2007.

[24] P. Kundur, *Power System Stability and Control*. New York, NY, USA: McGraw-Hill, 1994.

[25] J. Näsström. "State-of-the-art development platform for hydropower turbine governors," M.S. thesis, umeå university, Umeå, Sweden, 2017.

[26] M. Persson and P. Chen, "Kinetic Energy Estimation in the Nordic System," 2018 Power Systems Computation Conference (PSCC), 2018.